Synthesis of ordered large-scale ZnO nanopore arrays

G. Q. Ding, W. Z. Shen,[a] M. J. Zheng,[b] and D. H. Fan
Laboratory of Condensed Matter Spectroscopy and Opto-Electronic Physics, Department of Physics, Shanghai Jiao Tong University, 1954 Hua Shan Road, Shanghai 200030, China

(Received 13 November 2005; accepted 10 February 2006; published online 7 March 2006)

An effective approach is demonstrated for growing ordered large-scale ZnO nanopore arrays through radio-frequency magnetron sputtering deposition on porous alumina membranes (PAMs). The realization of highly ordered hexagonal ZnO nanopore arrays benefits from the unique properties of ZnO (hexagonal structure, polar surfaces, and preferable growth directions) and PAMs (controllable hexagonal nanopores and localized negative charges). Further evidence has been shown through the effects of nanorod size and thermal treatment of PAMs on the yielded morphology of ZnO nanopore arrays. This approach opens the possibility of creating regular semiconducting nanopore arrays for the application of filters, sensors, and templates. © *2006 American Institute of Physics*. [DOI: 10.1063/1.2182025]

ZnO is an important wide-band gap (3.37 eV) semiconductor with piezoelectric, pyroelectric, and photoconducting properties. ZnO has potential applications in numerous fields, including solar cells,[1] room-temperature ultraviolet lasers,[2] light emitting diodes,[3] field-emission devices,[4] gas sensors,[5] and photocatalysts.[6] Many kinds of ZnO nanostructures, such as nanorings,[7] nanobelts,[8] nanodots,[9] nanorods,[10,11] nanowires,[12,13] nanobridges,[14] and nanonails,[14] have been fabricated to improve performances and broaden applications. The variety of ZnO nanostructures benefits from the fact that ZnO has two polar surfaces [positively charged (0001)-Zn and negatively charged $(000\bar{1})$-O] and three fast growth directions ([0001], $[10\bar{1}0]$ and $[2\bar{1}\bar{1}0]$).[7,8] In this letter, we report a hitherto unexplored type of nanostructure, the large-scale ZnO nanopore arrays, taking advantage of charged surfaces and controllable sizes in hexagonal morphologies of both ZnO and self-organized porous alumina membranes (PAMs).

The basic idea comes from the unique properties of both ZnO and PAMs. A number of planes, which are composed of tetrahedrally coordinated Zn^{2+} and O^{2-} ions, stack alternately along the *c* axis to form the hexagonal ZnO grain. As Fig. 1(a) shows, the oppositely charged ions produce negatively charged $(000\bar{1})$-O and positively charged (0001)-Zn polar surfaces on either the top or the bottom of the ZnO grain.[7] The width and height of the ZnO grain are determined by the growth along the six equivalent side faces $\{10\bar{1}0\}$ and the *c* axis, respectively, and can be well controlled by the growth conditions during the magnetron sputtering.[15] On the other hand, PAMs are versatile templates, which have hexagonal nanopore arrays with controllable pore diameter of 20–200 nm, interpore spacing 50–400 nm, and thickness 0.1–200 μm.[16–21] Each hexagonal nanopore is formed by six hexagonal amorphous alumina nanorods [see Fig. 1(b)], where negative charges localize at the intermediate part of the PAM top surfaces due to the inhomogeneous distribution of anion species ($C_2O_4^{2-}$ and OH^-).[22,23]

During the deposition of ZnO grains on PAMs with Si substrates, these localized negative charges will attract Zn^{2+} ions, resulting in the ZnO nucleation and growth along the preferable directions at the PAM top surfaces, rather than onto the Si substrates through PAM nanochannels. This kind of nucleation process at the PAM top surfaces has been directly observed through field emission scanning electron microscope (FE-SEM).[24] Under certain growth conditions, the width of the grown ZnO grains on the PAM top surfaces can be very close to the size of the hexagonal amorphous alumina nanorods, and these six grains will form an hexagonal nanopore pattern identical to that of the PAMs, as shown schematically in Fig. 1(c). Therefore, well-ordered large-scale ZnO nanopore arrays can be fabricated on the top surfaces of the PAMs. With further deposition of ZnO grains, the O^{2-} ions on the surfaces will play the same role as the localized negative charges in PAMs, leading to the formation of the next round of ZnO nanopore array layer, i.e., multilayer growth of ZnO nanopore arrays [see Fig. 1(d)]. Figure 1(e) shows the cross-sectional view of multilayer ZnO nanopore arrays on top of a PAM on Si (100) substrate.

We prepare ultrathin PAMs through a typical two step anodizing procedure with high-purity (99.999%) aluminum foil as the anode in a 0.3 M oxalic acid electrolyte.[16,20] Throughout PAMs with controllable alumina nanorods (5–70 nm) were obtained by dissolving the barrier layers in phosphoric acid for different times. The free-standing ultrathin PAMs (150–500 nm) were washed and transferred onto Si substrates[21] for the ZnO deposition. ZnO layers were deposited on top of PAMs from bulk ZnO by radio-frequency (13.56 MHz) magnetron sputtering with a substrate temperature of 200 °C. The base pressure, deposition pressure, substrate–target distance, and the Ar flux were 2×10^{-4} Pa, 2 Pa, 4 cm, and 20 sccm, respectively, thus the depostion rate is less than 3 nm/min. The as-prepared specimens were cut to observe the cross section. The morphology and microstructure of the porous ZnO were observed by atomic force microscope (AFM) (Digital Instrument Multimode Nanoscope IIIa), FE-SEM (Philips XL30FEG), and high resolution transmission electron microscope (HRTEM) (JEOL JEM-2100F). The temperature-dependent micro-Raman and PL spectra were measured through Jobin Yvon LabRam HR 800UV system with a 325 nm He–Cd laser.

[a]Author to whom correspondence should be addressed; electronic mail: wzshen@sjtu.edu.cn
[b]Electronic mail: mjzheng@sjtu.edu.cn

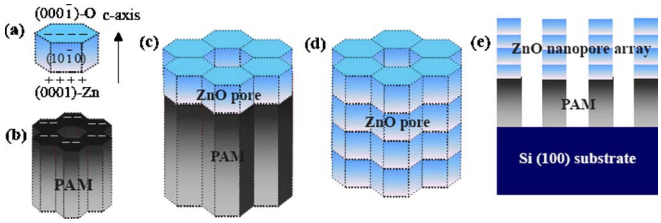

FIG. 1. (Color online) Schematic diagrams of growth mechanism for the ordered ZnO nanopore arrays by the aid of PAMs.

The inset of Fig. 2(a) shows the AFM image of a typical hexagonal PAM where a single hole is formed by six surrounding amorphous alumina nanorods. Since the size of ZnO grains can be well controlled by the Si substrate temperature during the magnetron sputtering deposition, we have employed the growth temperature of 200 °C to yield suitable ZnO grain width of ~30 nm[15] (intermediate size of the tested 5–70 nm alumina nanorods). For the PAM with the alumina nanorod size of ~30 nm (i.e., very close to the width of ZnO grains), the FE-SEM images shown in Fig. 2(a) (oblique view) and Fig. 2(b)) (top view) demonstrate that we have realized ZnO nanopore arrays on top of the PAM. The morphology of the ZnO nanopore arrays basically copies the highly ordered hexagonal pattern of the PAM, with the ZnO pore size, interpore distance, and thickness of ~70, 100, and 30 nm, respectively. The low magnification image displayed in Fig. 2(c) further indicates the growth of large-scale (>5 μm × 10 μm) ordered ZnO nanopore arrays.

The evidence for the synthesis of the ZnO nanopore arrays can be first observed in the energy-dispersive x-ray (EDX) spectra [Fig. 2(d)] taken on different layers of the specimen in Fig. 2(c). The EDX spectrum for the bottom PAM layer shows three peaks, i.e., the strong Si peak from the Si substrate, and the Al, O peaks due to the porous alumina layer. The absence of the Zn peak indicates that there is no ZnO deposited on either the sidewalls of the PAM or the Si substrate through the PAM nanochannels, consistent with

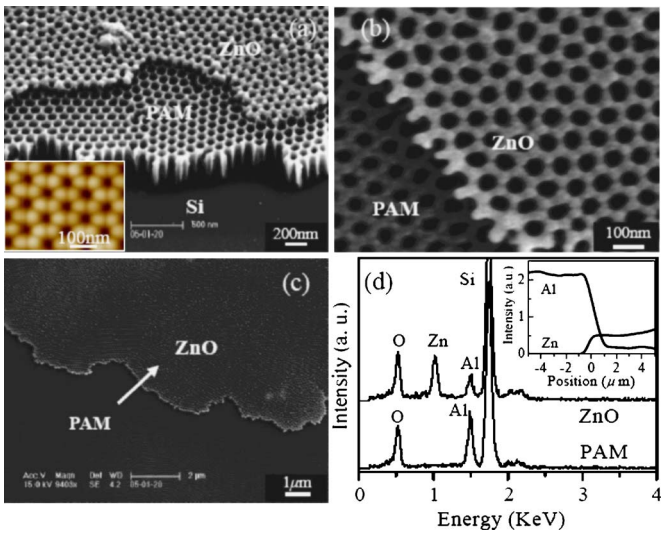

FIG. 2. (Color online) FE-SEM images of the: (a) oblique and (b) top view of the ordered ZnO nanopore array on top of PAM, (c) low magnification FE-SEM image of the obtained ZnO nanopore array on top of PAM, and (d) the EDX spectra of the bottom PAM layer and the top ZnO layer in (c). The inset in (a) is the AFM image of the original hexagonal PAM. The inset in (d) is the EDX compositional line profile along the arrow in (c) cross the interface (position 0 μm).

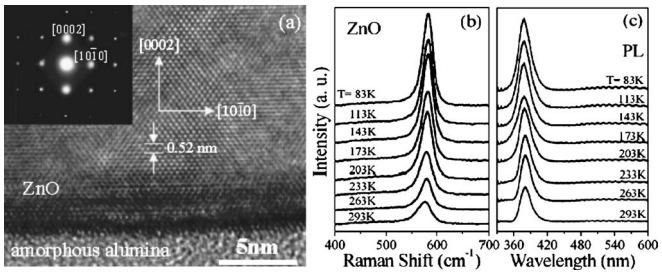

FIG. 3. (a) HRTEM image of the interface between the PAM and ZnO showing perfect crystalline ZnO on the amorphous alumina with a 3–4 nm ZnO transitional layer, the inset is the SAED pattern of the top ZnO layer, and (b) and (c) are the micro-Raman and PL spectra of the obtained highly ordered ZnO nanopore array.

the clean PAM nanochannels and Si substrate in the FE-SEM images [see e.g., Fig. 2(a)]. In contrast, the EDX spectrum for the top porous arrays does exhibit the Zn peak, verifying the formation of ZnO nanopores on the top surface of PAM. The EDX compositional line profile in the inset of Fig. 2(d) further supports the above arguments.

Second, HRTEM at the interface between the ZnO nanopore array and PAM [Fig. 3(a)] shows clean and perfect microstructure of the crystalline ZnO at the top surface of amorphous alumina with a very thin ZnO transitional layer (3–4 nm in thickness), confirming that high-quality ZnO nanopore arrays can be grown by the present technique. Both the lattice distance of 0.52 nm and the selected area electron diffraction (SAED) pattern shown in the inset demonstrate that the growth orientations of ZnO grains perpendicular and parallel to the top surfaces of PAMs are [0002] [10$\bar{1}$0] respectively. This kind of growth mechanism for the ZnO nanopore arrays agrees with the fast growth directions of ZnO.

Finally, micro-Raman [Fig. 3(b)] and photoluminescence (PL) [Fig. 3(c)] measurements have also been carried out to characterize the optical properties of the ordered ZnO nanopore arrays. Under the backscattering geometry of $Z(X,-)\bar{Z}$, the Raman spectra display one of the fundamental optical modes in wurtzite ZnO:[25] A_1 [longitudinal optical (LO)] at ~570 cm^{-1}, which redshifts with the increase of temperature. The absence of E_2 mode is associated with the oxygen deficiency.[26] In the PL spectra, as temperature is increased, the exciton emission in the UV region decreases in intensity, shifts to low energy, and increases in the full width at half maximum. The absence of an oxygen–vacancy-related green (~500 nm) luminescence band confirms again the high quality of the fabricated ZnO nanopore arrays.

Nevertheless, the realization of ordered ZnO nanopores is limited by the configuration (pore size and interpore spacing) of PAMs. For the PAMs with quite different alumina nanorod sizes from the width of ZnO grains, the deposited ZnO, as expected, displays totally different morphology under the same magnetron sputtering conditions. When the alumina nanorod size is ~60 nm, the ZnO nuclei grow up into more than one ZnO grain at the top of a single alumina nanorod, resulting in the formation of disordered ZnO nanopore arrays, as shown in Fig. 4(a). On the other hand, when the alumina nanorod is only ~10 nm, the attraction ability to Zn^{2+} ions will become weak due to the partial removal of the localized negative charges during the pore broadening process, and the ZnO grains cannot grow steadily on top of such a narrow alumina nanorod. As a result, ZnO migrates onto

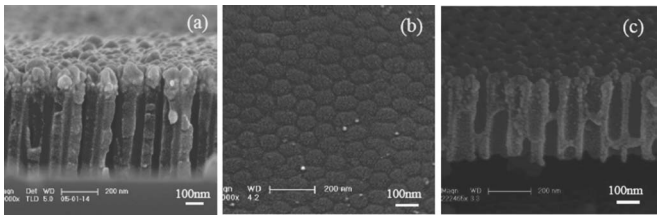

FIG. 4. (a) Disordered ZnO nanopore array on top of PAM, (b) ZnO nanodot array on the Si substrate after removal of PAM by 1% NaOH, and (c) ZnO deposited on PAM annealed at 900 °C for 2 h.

the bottom Si substrate through the PAM nanochannels to form hexagonal ZnO nanodot arrays, as revealed in Fig. 4(b).

Further evidence for the role of electrostatic attraction of Zn^{2+} ions by the localized negative charges in the formation of ordered ZnO nanopore arrays comes from our annealing experiments on PAMs. Figure 4(c) shows the cross-sectional view of the ZnO nanopore arrays deposited on the PAM annealed at 900 °C for 2 h. As we know, many $C_2O_4^{2-}$ in PAMs will decompose into CO_2 trapped in the lattice under an annealing temperature over 600 °C.[27] It is clear that the obtained ZnO nanopore arrays are not so ordered, and part of ZnO deposits into and clogs every nanochannel of the PAM due to the reduced electrostatic attraction.

It should be noted that, during the formation of a ZnO nanopore array layer, the growth along side faces ($\langle 10\bar{1}0\rangle$ directions) is restrained by the adjacent ZnO grains, limiting the growth along the $\langle 0001\rangle$ orientation with the height of the ZnO grains along the *c* axis to a certain value (~30 nm from Fig. 2). With the further continuous deposition of ZnO, the O^{2-} ions on the surface of the ZnO nanopore array layer will attract the Zn^{2+} ions (i.e., play the same role as the localized negative charges in PAMs), leading to the next round of ZnO nucleation and preferable direction growth. We therefore expect a multilayer growth of ZnO nanopore arrays [Fig. 1(d)] with the polar (0001)-Zn surface at the bottom to minimize the energy due to the polar surfaces and charges. Figures 5(a)–5(c) display the realized two, three, and four ZnO nanopore array layers with the same morphology and height (every layer ~30 nm), which clearly demonstrate the above expectation. Similar phenomena of layer-by-layer growth along the $\langle 0001\rangle$ orientations with a certain value of layer height have also been observed in the ZnO nanorings (~20 nm),[7] nanobelts (10–30 nm),[8] and helical nanorods (~15 nm).[28] The multilayer growth in nanostructures may be related to the orientation dependent growth energy.

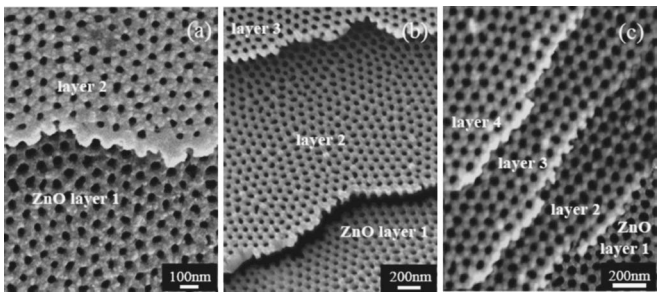

FIG. 5. FE-SEM images of (a) two, (b) three, and (c) four ZnO nanopore array layers with the same morphology and height.

Finally, we should point out that the as-synthesized samples (both single and multilayer) are composed of hexagonal ZnO nanopore arrays at a significant percentage (near 100%) of yield without any other formation of ZnO. The regular nanopores in the present ZnO nanostructure make it possible for the application of filters and sensors due to the large surface areas with polar charges. Furthermore, we can take away the ZnO nanopore array layers intact from the surfaces of PAMs to produce ZnO templates, which can even be transferred onto other substrates. Therefore, with the great advantages of semiconducting ZnO over the amorphous PAMs, the large-scale ZnO templates will be of great importance for future ZnO-based nanodevice applications.

Work was supported in part by the Natural Science Foundation of China under Contract Nos. 10125416 and 50572064, and the Shanghai Major Project Nos. 03DJ14003 and 05DJ14003.

[1] H. Rensmo, K. Keis, H. Lindstrolm, S. Soldergren, A. Solbrand, A. Hagfeldt, S. E. Lindquist, L. N. Wang, and M. Muhammed, J. Phys. Chem. B **101**, 2598 (1997).
[2] M. H. Huang, S. Mao, H. Q. Feick, H. Q. Yan, Y. Y. Wu, H. Kind, E. Weber, R. Russo, and P. D. Yang, Science **292**, 1897 (2001).
[3] D. K. Hwang, S. H. Kang, J. H. Lim, E. G. Yang, J. Y. Oh, J. H. Yang, and S. J. Park, Appl. Phys. Lett. **86**, 222101 (2005).
[4] D. Banerjee, S. H. Jo, and Z. F. Ren, Adv. Mater. (Weinheim, Ger.) **16**, 2028 (2004).
[5] S. T. Shishiyanu, T. S. Shishiyanu, and O. I. Lupan, Sens. Actuators B **107**, 379 (2005).
[6] K. Maeda, T. Takata, M. Hara, N. Saito, Y. Inoue, H. Kobayashi, and K. Domen, J. Am. Chem. Soc. **127**, 8286 (2005).
[7] X. Y. Kong, Y. Ding, R. S. Yang, and Z. L. Wang, Science **303**, 1348 (2004).
[8] Z. W. Pan, Z. R. Dai, and Z. L. Wang, Science **291**, 1947 (2001).
[9] W. L. Xu, M. J. Zheng, G. Q. Ding, and W. Z. Shen, Chem. Phys. Lett. **411**, 37 (2005).
[10] X. D. Wang, C. J. Summers, and Z. L. Wang, Nano Lett. **4**, 423 (2004).
[11] B. Liu and H. C. Zheng, J. Am. Chem. Soc. **125**, 4430 (2003).
[12] Y. Ding, P. X. Gao, and Z. L. Wang, J. Am. Chem. Soc. **126**, 2066 (2004).
[13] E. C. Greyson, Y. Babayan, and T. W. Odom, Adv. Mater. (Weinheim, Ger.) **16**, 1348 (2004).
[14] J. Y. Lao, J. Y. Huang, D. Z. Wang, and Z. F. Ren, Nano Lett. **3**, 235 (2003).
[15] E. Mirica, G. Kowach, P. Evans, and H. Du, Cryst. Growth Des. **4**, 147 (2004).
[16] H. Masuda and K. Fukuda, Science **268**, 1466 (1995).
[17] H. Chik and J. M. Xu, Mater. Sci. Eng., R. **43**, 103 (2004).
[18] Y. Lei and W. K. Chim, Chem. Mater. **17**, 580 (2005).
[19] K. L. Hobbs, P. R. Larson, G. D. Lian, J. C. Keay, and M. B. Johnson, Nano Lett. **4**, 167 (2004).
[20] S. Y. Jeong, J. Y. Kim, H. D. Yang, B. N. Yoon, S. H. Choi, H. K. Kang, C. W. Yang, and Y. H. Lee, Adv. Mater. (Weinheim, Ger.) **14**, 1172 (2003).
[21] G. Q. Ding, M. J. Zheng, W. L. Xu, and W. Z. Shen, Nanotechnology **16**, 1285 (2005).
[22] K. Nielsch, J. Choi, K. Schwirn, R. B. Wehrspon, and U. Gösele, Nano Lett. **2**, 677 (2002).
[23] J. Choi, Y. Luo, R. B. Wehrspohn, R. Hillebrand, J. Schilling, and U. Gösele, J. Appl. Phys. **94**, 4757 (2003).
[24] J. S. Jie, G. Z. Wang, Q. T. Wang, Y. M. Chen, X. H. Han, X. P. Wang, and J. G. Hou, J. Phys. Chem. B **108**, 11976 (2004).
[25] Y. Zhang, H. B. Jia, R. M. Wang, C. P. Chen, X. H. Luo, D. P. Yu, and C. L. Lee, Appl. Phys. Lett. **83**, 4631 (2003).
[26] G. J. Exarhos and S. K. Sharma, Thin Solid Films **270**, 27 (1995); X. L. Xu, S. P. Lau, J. S. Chen, G. Y. Chen, and B. K. Tay, J. Cryst. Growth **223**, 201 (2001).
[27] W. L. Xu, M. J. Zheng, S. Wu, and W. Z. Shen, Appl. Phys. Lett. **85**, 4364 (2004).
[28] Z. R. Tian, J. A. Voigt, J. Liu, B. Mckenzie, and M. J. Mcdermott, J. Am. Chem. Soc. **124**, 12954 (2002).